Crystallization and Precursors during Fast Short-Term Shear

Luigi Balzano,[†,||] Sanjay Rastogi,[†,§,||] and Gerrit W. M. Peters*[,‡,||]

Department of Chemical Engineering and Department of Mechanical Engineering, Eindhoven University of Technology, P.O. Box 513, 5600 MB Eindhoven, The Netherlands; Institute of Polymer Technology and Materials Engineering (IPTME), Loughborough University, Loughborough, LE11 3TU, United Kingdom; and Dutch Polymer Institute (DPI), PO Box 902, 5600 AX Eindhoven, The Netherlands

Received September 24, 2008; Revised Manuscript Received January 12, 2009

ABSTRACT: This paper deals with structural and morphological developments during flow-induced crystallization of molten isotactic polypropylene (iPP). Several authors have invoked the formation of precursors in the early stages of this process. However, it is not clear whether these precursors can be generated and can crystallize already during flow. We address this issue using X-ray scattering (SAXS and WAXD) with a high image capturing rate *during* and *immediately after* a strong shear pulse to the undercooled melt. Eventually, we provide the first in situ evidence of formation of flow-induced precursors (FIPs) of crystallization generated applying shear to a *fast crystallizing melt of flexible macromolecules*, like iPP. Moreover, it is shown that a rheological classification can be used to define the flow conditions promoting FIPs formation. In fact, when molecular stretch is achieved, we found that shear rate is the parameter dominating the formation of structures *during* shear. When the shear rate is high enough, crystals with a high degree of orientation are formed during a brief shear pulse. Whereas, for low shear rates, crystalline structures do not develop during a brief shear pulse. However, the equatorial streak of intensity in SAXS points to the formation of high density domains with fibrillar morphology. These dense and noncrystalline scatterers are metastable precursors of crystallization. After cessation of flow, they nucleate and assist the radial growth of stacks of lamellae. Eventually, this sequence of events leads to the well-known shish-kebab morphology.

1. Introduction

Polymeric materials with a regular molecular structure have the ability to partially crystallize, forming a two phase system where crystals are dispersed in an amorphous matrix.[1−5] Crystallinity affects many of the material properties, from mechanical to optical.[1−9] Semicrystalline polymers are stiffer than amorphous and tend to be opaque. However, universal rules are difficult to establish because these materials exhibit a processing−structure relation; i.e., the final properties are affected by the processing conditions. Both temperature and flow history can alter the crystallization behavior. Flow can increase the crystallization rate by decades[10−15] and, in addition, can dramatically change the crystalline morphology.[16−21] In quiescent or quasi-quiescent conditions, morphology is dominated by spherulites, three-dimensional assemblies of randomly oriented folded chain lamellae.[22] For strong enough flows, spherulites are replaced by shish-kebabs, composite crystallites with an extended chain fibrillar core (shish) dressed with disk-like folded chain lamellae (kebabs).[23−29] The origin of the shish-kebab morphology is the topic of a long-standing discussion[28,30−34] that begun around the 1960s. It is known that stretch of the longest (highest molecular weight) molecules in a undercooled melt promotes shish-kebab formation, but the events in the early stages of the process are not yet fully clarified and certainly not quantified, an important issue for modeling. Several authors invoked the formation of precursors of crystallization,[31,35−40] i.e., an intermediate phase directing the subsequent developments of the crystallization process. For instance, flow-induced precursors (FIPs) were observed by Lee and Schultz[41] studying fiber spinning of poly(ethylene terephthalate) (PET). These authors describe the flow-induced formation of an "oriented mesophase" that, in the early stages, is amorphous and eventually crystallizes. The mesophase evolves quickly, and it could be characterized with X-rays only ex situ after quenching the fibers to a no-molecular mobility temperature before the onset of crystallization. Such a protocol suits a slow crystallizing polymer like PET whereas it is hard to apply to fast crystallizing polymers such as isotactic polypropylene (iPP). In the latter case, the study of FIPs is often carried out, in situ, applying a pulse of shear and following the evolution of the system after cessation of flow.[30,36,38,42−46] This short-term shear protocol offers the advantage of an easy characterization of the flow conditions assuming a melt-like rheological behavior based on the "hope" that no noticeable material change occurs during flow. Recently, we studied FIPs in a bimodal polyethylene (PE) melt with this protocol.[35] It was found that FIPs are bundles of stretched chains that, although not crystalline, have a density higher than the melt. In agreement with the classical view on crystallization,[47] after cessation of flow, a selection takes place among FIPs: those exceeding some critical dimensions transform into crystals, whereas the remainders dissolve into the melt. The ratio between crystallizing and dissolving FIPs and the rate of crystallization and dissolution are fixed by the temperature; high temperature favors dissolution, and low temperature favors crystallization. The present paper addresses the formation of FIPs *during* the flow period in short-term shear. The aim is to answer the following questions: When are actually FIPs created and when do they crystallize, during or after cessation of flow? The answers are some novel observations of the early stages of flow-induced crystallization. Because of the fast dynamics of FIPs, this investigation is only possible with the use of synchrotron X-ray scattering with a high flux of photons allowing for a short sampling time (∼0.3 s).

* To whom correspondence should be addressed.
† Department of Chemical Engineering, Eindhoven University of Technology.
‡ Department of Mechanical Engineering, Eindhoven University of Technology.
§ Loughborough University.
|| Dutch Polymer Institute.

10.1021/ma802169t CCC: $40.75
Published on Web 02/20/2009

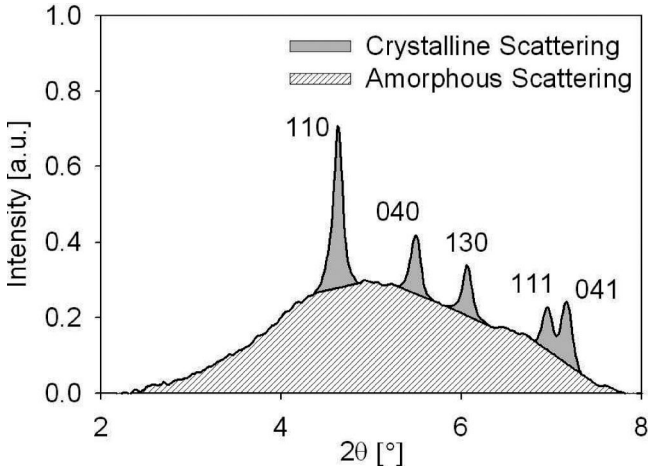

Figure 1. Example of the procedure to separate crystalline and amorphous scattering. The Miller indices of the scattering reflections are indicated as well.

Table 1. Specification of the iPP used in This Work

	M_w [kg/mol]	M_w/M_n	tacticity [% mmmm]	T_m [°C]
15M10	350	5.6	96.2	161

2. Materials and Methods

2.1. Materials. The polymer used in this work is a commercial homopolymer grade of isotactic polypropylene (iPP). The material, labeled 15M10, was obtained from SABIC Europe (Geleen, The Netherlands) and contained no other additives than stabilizers. The specifications of the material are reported in Table 1.

2.2. X-ray Characterization. Small-angle X-ray scattering (SAXS) was performed at the beamline ID02 of the European Synchrotron Radiation Facility (ESRF, Grenoble). The samples were irradiated with a wavelength $\lambda = 0.995$ Å, and two-dimensional images were recorded using a Frelon detector, with a resolution of 1024 × 1024 pixels and a pixel size of 164 μm, placed at about 6.5 m from the sample. After subtraction of the scattering of the empty sample holder, images were integrated to obtain the scattered intensity (I) as a function of the modulus of the scattering vector $q = (4\pi/\lambda) \sin \theta$, where 2θ is the scattering angle.[48,49] The intensity I^{SAXS} as a function of time was obtained integrating $I(q)$ over the whole accessible q range: $I^{SAXS}(t) = \int_{q_{min}}^{q_{max}} I(q;t)\, dq$.

Wide-angle X-ray diffraction (WAXD) was performed at the beamline ID11 of the ESRF. Experiments were carried out with a wavelength $\lambda = 0.508$ Å and a sample-to-detector distance of about 32 cm. The images were recorded with a two-dimensional Frelon detector with a resolution of 512 × 512 pixels (pixel size ≅ 190 μm). After correction for spatial distortions and scattering of the empty sample holder, the images were integrated to obtain the intensity distribution as a function of the scattering angle 2θ. These one-dimensional profiles were used to calculate crystallinity. For this purpose, the scattering of the amorphous component (I_A) underneath crystalline peaks (I_C) was approximated with a straight line (see Figure 1). This simplified procedure is expected to give trustworthy results at low crystallinity, in the order of ∼10%.[50] Crystallinity (x) was determined as

$$x = 100\frac{I_C}{I_C + I_A} \quad (1)$$

2.3. Shear Experiments. Shear experiments were performed in combination with SAXS and WAXD using a Linkam CSS-450 shear cell where the original glass plates were replaced with Kapton. When shearing, a metal spoke of the rotating plate lies periodically in front of the incoming beam, and the corresponding (dark) scattering images are discarded from analysis.

Table 2. Deborah Numbers for the Flow-Induced Crystallization Experiments

	De_O	De_S
60 s^{-1}/3 s	6×10^3	60
90 s^{-1}/2 s	9×10^3	90
180 s^{-1}/1 s	1.8×10^4	180

3. Results and Discussion

Shear flow promotes orientation and stretch of polymer molecules in the melt.[20,21,51−53] The effect of shear on the configuration of the molecules is often classified with the Deborah number (De).[51] With the shear rate $\dot{\gamma}$, the disengagement time (relaxation time for orientation) of the longest molecules τ_D and the chain retraction time (relaxation time for stretch) τ_S, the Deborah number for orientation is defined as $De_O = \tau_D\dot{\gamma}$ and the Deborah number for stretch as $De_S = \tau_S\dot{\gamma}$. During a shear, the longest molecules orient when $De_O \gg 1$ and $De_S < 1$ and stretch when $De_O \gg 1$ and $De_S \gg 1$. The ratio τ_D/τ_S equals the number of entanglements per chain Z[54−56] (neglecting a factor of the order of unity). In an entangled polymer melt, $Z \gg 1$ and thus $De_O \gg De_S$; i.e., chain orientation is attained at shear rates much lower than chain stretch. For the iPP under consideration, $Z \cong 100$ and, therefore, $De_O \cong 100De_S$. To induce a large amount of FIPs, detectable with X-rays, a shear regime inducing molecular stretch is required. Therefore, the experimental conditions are chosen such that $De_S \gg 1$. For the iPP considered, rheological analysis[57] suggests that $\tau_D \cong 100$ s and $\tau_S \cong 1$ s at 145 °C, and therefore, shear rates of 60, 90, and 180 s^{-1} suite our experimental requirements. The shear time (t_S) is varied accordingly to keep the total strain $\gamma = \dot{\gamma}t_S = 180$. The selected shear conditions are summarized in Table 2. WAXD patterns acquired at a rate of 3 images/s during and immediately after short-term shear at 145 °C are shown in Figure 2. In these figures, as in the rest of the paper, the time $t = 0$ corresponds to cessation of the flow. For a shear of 60 s^{-1} for 3 s, no crystalline reflection is detected during shear ($t < 0$). In contrast, for both 90 s^{-1} for 2 s and 180 s^{-1} for 1 s, diffraction of highly oriented iPP crystals (i.e., arched 110 and 040 reflections) is visible already during the shear. This indicates that, when the shear rate is strong enough, the melt transforms into a suspension of highly oriented crystalline structures already during the brief shear. Structural information on the crystals, obtained analyzing the diffracted intensity, is given in Figure 3. Here, we see that, during shear, at $t = -0.3$ s ∼0.1% of α-phase crystals are formed at 90 s^{-1}, while at 180 s^{-1} crystallinity reaches ∼2% and next to the α-phase also γ-phase crystals are present (indicated by the broad 117). As shown in the right part of Figure 3, this difference in polymorphism is retained also at long times after cessation of shear (at $t = 30$ s, for instance). For a shear pulse of 60 s^{-1} for 3 s, the lack of crystalline diffraction during shear does not necessarily imply the absence of structure in the melt. To investigate this point further the experiment is studied in more detail, acquiring 3 SAXS images/s. As shown in Figure 4, during shear a streak of intensity appears at the equator. Such an observation points to the formation of fibrillar domains where density is higher than the surroundings. Therefore, the melt does exhibit structures before the onset of crystallization. These high-density structures are precursors of crystallization. They form due to stretching of the molecular network ($De_S \gg 1$) and, as demonstrated by the appearance of WAXD peaks and SAXS meridional lobes, crystallize and assist the nucleation of stacks of lamellae (kebabs) after cessation of the flow. The intensity scattered in the meridional region exceeds the intensity in the equatorial region about 3 s after shear (see Figure 5). The crossover between meridional and equatorial intensity indicates the transition from the fibrillar morphology of FIPs in the early stages to a well-developed shish-kebab morphology. The growth

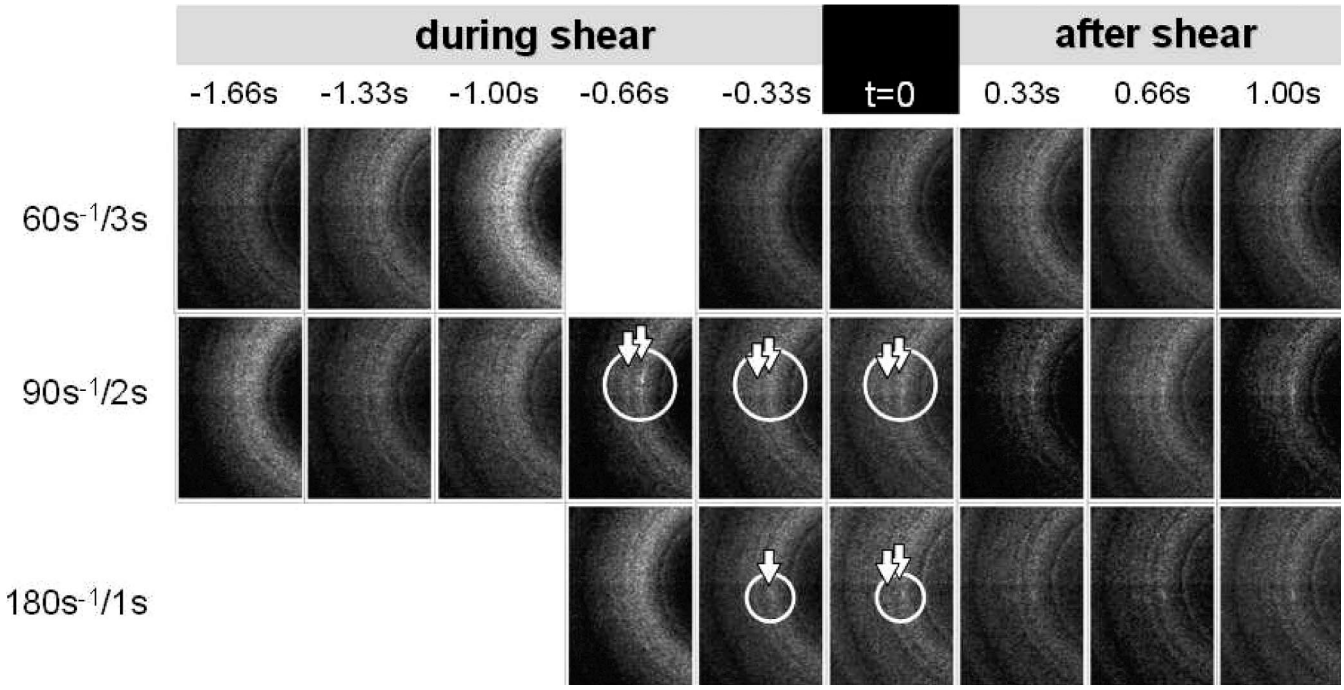

Figure 2. Equatorial region of WAXD patterns during and after short-term shear at 145 °C with $\gamma = 180$. Flow direction is vertical. To enhance visibility of the arched reflections at low crystallinity, only part of the pattern is shown. Shear starts at $t = -3$ s for 60 s^{-1}, at $t = -2$ s for 90 s^{-1}, and at $t = -1$ s for 180 s^{-1}. The arrows indicate arched crystalline reflections.

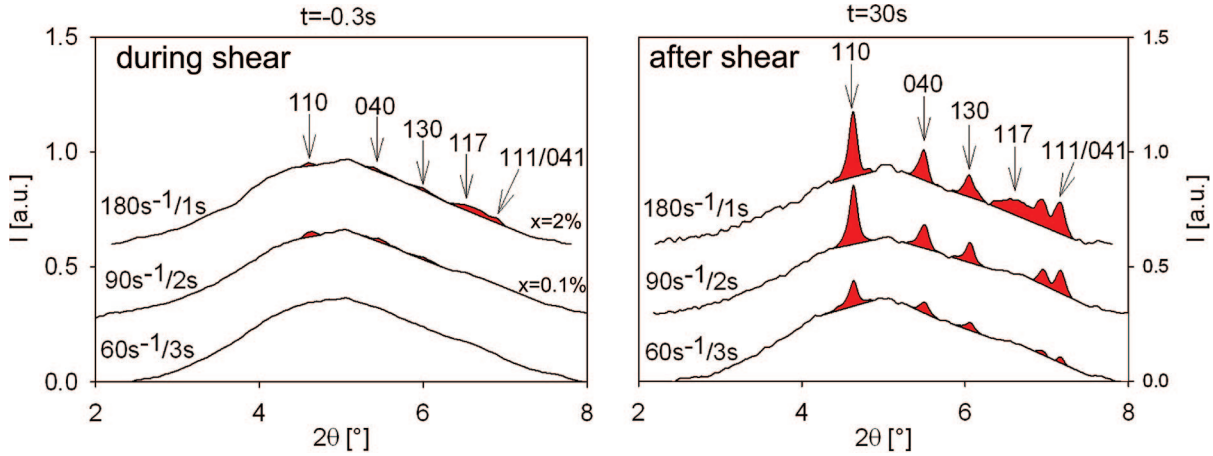

Figure 3. WAXD integrations during and after application of shear at 145 °C. Filled area represents crystalline diffraction (I_C in formula 1).

of kebabs after shear raises crystallinity for all flow conditions. Figure 6 illustrates the effect that $\dot{\gamma}$ and t_S exert on the crystallization rate after shear at 145 °C. Higher $\dot{\gamma}$ leads to a higher final crystallinity. More details on the crystallization kinetics after cessation of shear can be obtained defining the degree of space filling developed after cessation of flow:

$$\Phi(t) = \frac{x(t) - x_0}{x_\infty - x_0} \tag{2}$$

where $x(t)$ is the crystallinity at the time t, x_0 is the crystallinity present at the time $t = 0$ (i.e., generated during shear), and x_∞ is the saturation level attained by crystallinity at long times (the values, obtained from the data of Figure 6, are given in Table 3). We distinguish between space filling during and after flow because the nucleation and growth mechanism of the crystals can be different. $\Phi(t)$ can be described with the Avrami equation:[58−60]

$$\Phi(t) = 1 - \exp(-kt^n) \tag{3}$$

with k being a rate constant and n the Avrami exponent that indicates the geometry of the growing crystallites. Equation 3 can be rewritten as

$$\ln\{-\ln[1 - \Phi(t)]\} = \ln(k) + n \ln(t) \tag{4}$$

Therefore, $\ln\{-\ln[1 - \Phi(t)]\}$ as a function of $\ln(t)$ (the so-called Avrami plot) is a straight line with slope n. The Avrami plot, for the crystallization following the cessation of shear, is shown in Figure 7. The lines are obtained fitting eq 4 on the data. The fitted parameters are given in Table 3. Independent of flow conditions, $n \cong 1.36 \pm 0.02$ indicates that, in all cases, space filling occurs because of the growth of both fibrillar and disklike crystals. It is remarkable that the Avrami equation provides a good description of the crystallization data only when it accounts for the crystallinity generated already during shear (x_0 in eq 2). Although x_0 can be small, we found that it has large influence on the result.

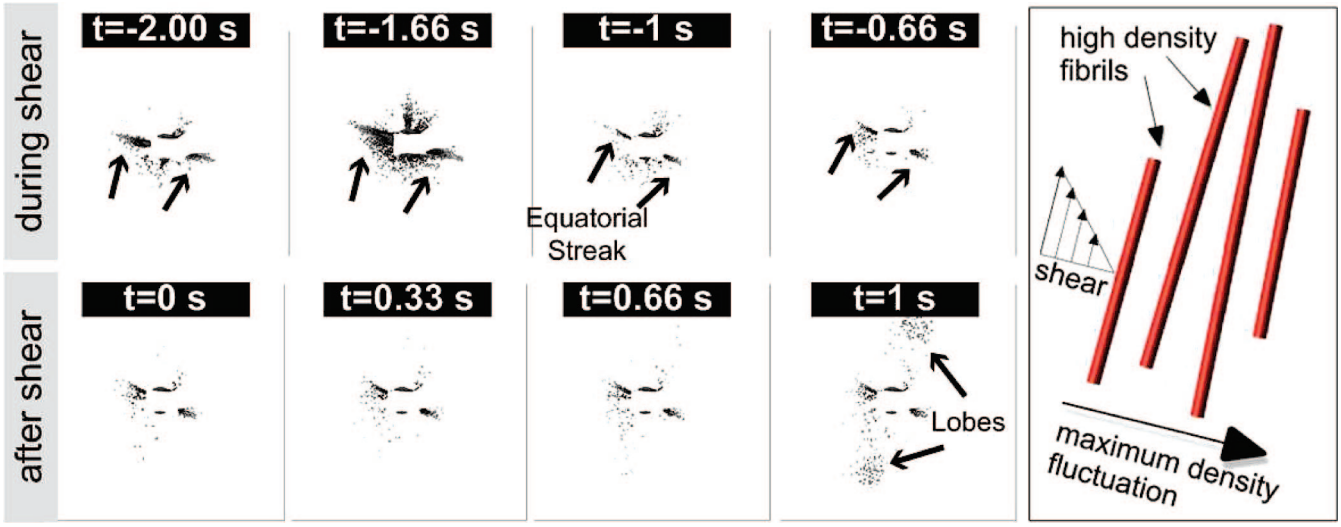

Figure 4. SAXS patterns during and immediately after short-term shear at 145 °C with 60 s^{-1}/3 s. On the right, a schematic drawing of a suspension of aligned high-density fibrils.

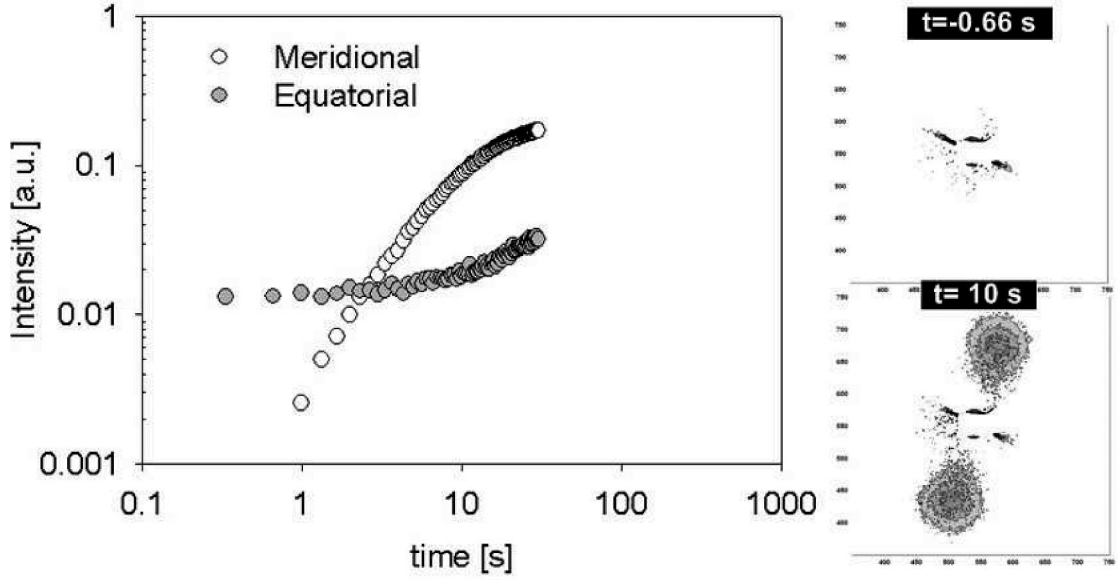

Figure 5. SAXS meridional and equatorial intensities at 145 °C as a function of time after the application of shear (60 s^{-1}/3 s).

Table 3. Parameters Obtained Fitting Eq 4 on the Data of Figure 7

	x_∞ [%]	x_0 [%]	n	k [s^{-n}]
60 s^{-1}/3 s	14.5	0	1.34	2.70×10^{-3}
90 s^{-1}/2 s	16.2	0.1	1.37	6.78×10^{-3}
180 s^{-1}/1 s	18.8	2	1.38	8.20×10^{-3}

4. Conclusions

Several authors have invoked the formation of precursors in the early stages of flow-induced crystallization. However, it is not clear whether these precursors can be generated and can crystallize already during flow. To solve this issue, we studied the early stages of the flow-induced crystallization of iPP from the melt, *during* and *immediately after* the application of a pulse of shear promoting molecular stretch ($De_S \gg 1$). At 145 °C, with a total strain $\gamma = 180$, X-ray scattering images (SAXS and WAXD), acquired at a rate of 3 images/s, suggest that shear rate is the dominant parameter for structure development during flow. We show that when the shear rate is high enough (≥90 s^{-1}), crystalline structures are nucleated already *during* shear. We observe the formation of up to 2% of crystals with a high degree of orientation. These crystals assist the nucleation of the rest of the molecules and thus direct subsequent developments in structure and morphology. On the other hand, at lower shear

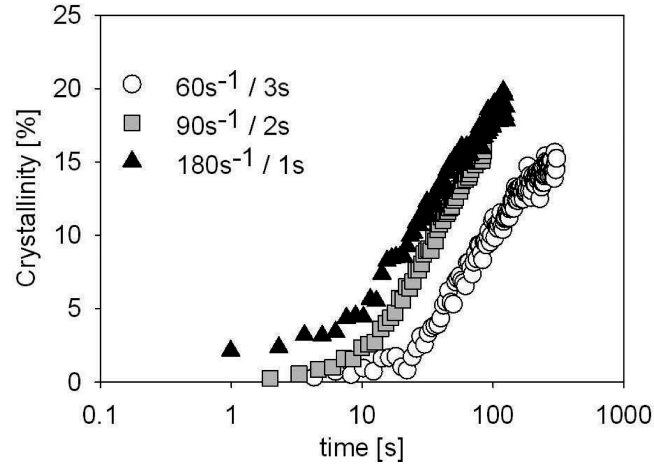

Figure 6. Increase in crystallinity at 145 °C after the application of 180 strain units with different flow rates.

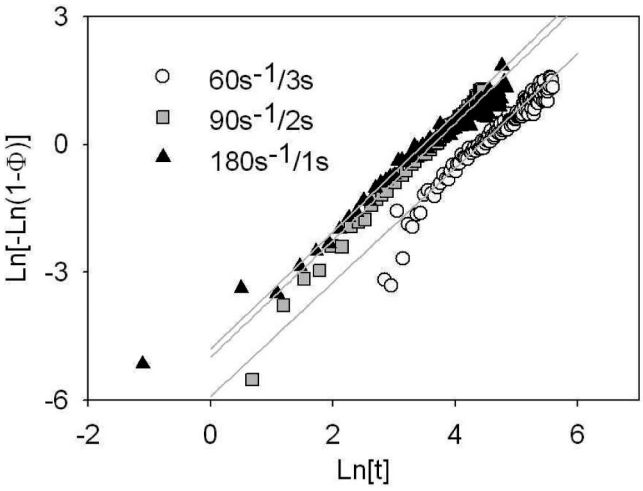

Figure 7. Avrami plot constructed with crystallinity data after short-term shear at 145 °C.

rates (for instance 60 s^{-1}), only metastable precursors of crystallization are generated *during* flow. To our knowledge, this is the first in situ evidence of precursors of crystallization generated applying shear to a fast crystallizing melt of flexible macromolecules. These precursors, with fibrillar morphology, have a density higher than the melt and no crystallinity. When flow stops, they crystallize and, similar to the crystals generated during shear, assist the crystallization of the rest of the polymer, leading to the formation of shish-kebabs.

Acknowledgment. The authors acknowledge ESRF for granting the beamtime and the personnel of ID11 and ID02 of the ESRF for providing valuable help during the X-ray experiments. This work is part of the Research Programme of the Dutch Polymer Institute (DPI), PO Box 902, 5600 AX Eindhoven, The Netherlands, project no. #132.

References and Notes

(1) Schrauwen, B. A. G.; Breemen, L. C. A. v.; Spoelstra, A. B.; Govaert, L. E.; Peters, G. W. M.; Meijer, H. E. H. *Macromolecules* **2004**, *37*, 8618–8633.
(2) Kristiansen, M.; Werner, M.; Tervoort, T.; Smith, P.; Blomehofer, M.; Schmidt, H. W. *Macromolecules* **2003**, *36*, 5150–5156.
(3) Smith, P.; Lemstra, P. J. *J. Mater. Sci.* **1980**, *15*, 505–514.
(4) Baastiansen, C. W. M. Oriented structures based on flexible polymers. PhD Thesis, Eindhoven University of Technology, **1991**.
(5) Govaert, L. E. Deformation behavior of oriented polyethylene fibers. PhD Thesis, Eindhoven University of Technology, **1990**.
(6) Meer, D. W. v. d.; Pukanszky, B.; Vancso, G. J. *J. Macromol. Sci., Phys.* **2002**, *41*, 1105–1119.
(7) Bashir, Z.; Odell, J. A.; Keller, A. *J. Mater. Sci.* **1984**, *19*, 3713–3725.
(8) Wallner, G. M.; Resch, K.; Teichert, C.; Gahleitner, M.; Binder, W. *Monatsh. Chem.* **2006**, *137*, 887–897.
(9) Michler, G. H.; Baltá-Calleja, F. J. *Mechanical Properties of Polymers Based on Nanostructure and Morphology*; CRC: Boca Raton, FL, 2005.
(10) Coppola, S.; Balzano, L.; Gioffredi, E.; Maffettone, P. L.; Grizzuti, N. *Polymer* **2004**, *45*, 3249–3256.
(11) Lagasse, R. R.; Maxwell, B. *Polym. Eng. Sci.* **1976**, *16*, 189.
(12) Heeley, E. L.; Morgovan, A.; Bras, W.; Dolbnya, I. P.; Gleeson, A. J.; Ryan, A. J. *PhysChemComm* **2002**, *5*, 158–160.
(13) Kumaraswamy, G.; Kornfield, J. A.; Yeh, F.; Hsiao, B. S. *Macromolecules* **2002**, *35*, 1762–1769.
(14) Nogales, A.; Hsiao, B. S.; Somani, R. H.; Srinivas, S.; Tsou, A. H.; Balta-Calleja, F. J.; Ezquerra, T. *Polymer* **2001**, *42*, 5247–5256.
(15) Devaux, N.; Monasse, B.; Haudin, J. M.; Moldenaers, P.; Vermant, J. *Rheol. Acta* **2004**, *43*, 210–222.
(16) Keller, A.; Kolnaar, H. W. H. *Flow Induced Orientation and Structure Formation*; VCH: New York, 1997; Vol. *18*.
(17) Hsiao, B. S.; Yang, L.; Somani, R. H.; Avila-Orta, C. A.; Zhu, L. *Phys. Rev. Lett.* **2005**, *94*, 117802.
(18) Hobbs, J. K.; Humphris, A. D. L.; Miles, M. J. *Macromolecules* **2001**, *34*, 5508–5519.
(19) Sakellarides, S. L.; McHugh, A. J. *Rheol. Acta* **1987**, *26*, 64–77.
(20) Seki, M.; Thurman, D. W.; Oberhauser, J. P.; Kornfield, J. A. *Macromolecules* **2002**, *35*, 2583–2594.
(21) Somani, R. H.; Hsiao, B. S.; Nogales, A.; Srinivas, S.; Tsou, A. H.; Sics, I.; Balta-Calleja, F. J.; Ezquerra, T. A. *Macromolecules* **2000**, *33*, 9385–9394.
(22) Basset, D. C.; Franck, F. C.; Keller, A. *Philos. Trans. R. Soc. London A* **1994**, *348*, 29–43.
(23) Binsbergen, F. L. *Nature (London)* **1966**, *211*, 516–517.
(24) Pennings, J.; Kiel, A. M. *Kolloid Z. Z. Polym.* **1965**, *205*, 160.
(25) Ogino, Y.; Fukushima, H.; Matsuba, G.; Takahashi, N.; Nishida, K.; Kanaya, T. *Polymer* **2006**, *47*, 5669–5677.
(26) Wang, Z. G.; Hsiao, B. S.; Sirota, E. B.; Srinivas, S. *Polymer* **2000**, *41*, 8825–8832.
(27) Yamazaki, S.; Watanabe, K.; Okada, K.; Yamada, K.; Tagashira, K.; Toda, A.; Hikosaka, M. *Polymer* **2005**, *46*, 1685–1692.
(28) Kimata, S.; Sakurai, T.; Nozue, Y.; Kasahara, T.; Yamaguchi, N.; Karino, T.; Shibayama, M.; Kornfield, J. A. *Science* **2007**, *316* (5827), 1014–1017.
(29) Hill, M. J.; Barham, P. J.; Keller, A. *Colloid Polym. Sci.* **1980**, *258*, 1023–1037.
(30) Janeschitz-Kriegl, H.; Eder, G. *J. Macromol. Sci., Part B* **2007**, *46*, 591–601.
(31) Kanaya, T.; Takayama, Y.; Ogino, Y.; Matsuba, G.; Nishida, K. *Lect. Notes Phys.* **2007**, *714*, 87–96.
(32) McHugh, A. J. *Polym. Eng. Sci.* **1982**, *22*, 15–26.
(33) Somani, R. H.; Yang, L.; Zhu, L.; Hsiao, B. S. *Polymer* **2005**, *46*, 8587–8623.
(34) Yamazaki, S.; Hikosaka, M.; Toda, A.; Wataoka, I.; Gu, F. *Polymer* **2002**, *43*, 6585–6593.
(35) Balzano, L.; Kukalyekar, N.; Rastogi, S.; Peters, G. W. M.; Chadwick, J. C. *Phys. Rev. Lett.* **2008**, *100*, 048302.
(36) Azzurri, F.; Alfonso, G. C. *Macromolecules* **2005**, *38*, 1723–1728.
(37) Somani, R. H.; Yang, L.; Hsiao, B. S.; Agarwal, P. K.; Fruitwala, H. A.; Tsou, A. H. *Macromolecules* **2002**, *35*, 9096–9104.
(38) Yang, L.; Somani, R. H.; Sics, I.; Hsiao, B. S.; Kolb, R.; Lohse, D. *J. Phys.: Condens. Matter* **2006**, *18*, 2421–2436.
(39) Mahendrasingam, A.; Martin, C.; Fuller, W.; Blundell, D. J.; Oldman, R. J.; MacKerron, D. H.; Harvie, J. L.; Riekel, C. *Polymer* **2000**, *41*, 1217–1221.
(40) Ezquerra, T.; Lopez-Cabarcos, E.; Hsiao, B. S.; Baltá-Calleja, F. J. *Phys. Rev. E* **1996**, *54*, 898–991.
(41) Lee, K.-G.; Schultz, J. M. *Polymer* **1993**, *34*, 4455–4470.
(42) Keum, J. K.; Zuo, F.; Hsiao, B. S. *J. Appl. Crystallogr.* **2007**, *40*, 48–51.
(43) Jerschow, P.; Janeschitz-Kriegl, H. *Int. Polym. Process.* **1997**, *12*, 72–77.
(44) Van der Beek, M. H. E.; Peters, G. W. M.; Meijer, H. E. H. *Macromolecules* **2006**, *39*, 1805–1814.
(45) Pogodina, N. V.; Winter, H. H.; Srinivas, S. *J. Polym. Sci., Part B: Polym. Phys.* **1999**, *37*, 3512–3519.
(46) Elmoumni, A.; Gonzalez-Ruiz, R. A.; Coughlin, E. B.; Winter, H. H. *J. Chem. Phys.* **2005**, *206*, 125–134.
(47) Muthukumar, M. *Adv. Chem. Phys.* **2004**, 128.
(48) Stribeck, N. *X-ray Scattering of Soft Matter*; Springer Laboratory: **2007**.
(49) Balta-Calleja, F. J.; Vonk, C. G. *X-ray Scattering of Synthetic Polymers*; Elsevier: Amsterdam, 1989.
(50) Kumaraswamy, G.; Verma, R. K.; Kornfield, J. A.; Yeh, F.; Hsiao, B. S. *Macromolecules* **2004**, *37*, 9005–9017.
(51) van Meerveld, J.; Peters, G. W. M.; Hutters, M. *Rheol. Acta* **2004**, *44*, 119–134.
(52) Dukovski, I.; Muthukumar, M. *J. Chem. Phys.* **2003**, *118*, 6648–6655.
(53) Somani, R. H.; Yang, L.; Hsiao, B. S. *Physica A* **2002**, *304*, 145–157.
(54) Dealy, J. M.; Larson, R. G. *Structure and Rheology of Molten Polymers*; Hanser Gardner Pubns: Cincinnati, 2006.
(55) Doi, M.; Edwards, S. F. *The Theory of Polymer Dynamics*; Clarendon Press: Oxford, 1986.
(56) McLeish, T. C. B. *Adv. Phys.* **2002**, *51*, 1379–1527.
(57) Swartjes, F. H. M. Stress induced crystallization in elongational flow. PhD Thesis, Eindhoven University of Technology, **2001**.
(58) Avrami, M. *J. Chem. Phys.* **1939**, *7*, 1103–1112.
(59) Avrami, M. *J. Chem. Phys.* **1940**, *8*, 212–224.
(60) Avrami, M. *J. Chem. Phys.* **1941**, *9*, 177–184.

MA802169T